

# How to measure diffusional decoherence in multimode rubidium vapor memories?

Radosław Chrapkiewicz,\* Wojciech Wasilewski, and Czesław Radzewicz

*Institute of Experimental Physics, University of Warsaw, ul. Hoża 69, 00-681, Warsaw, Poland*

(Dated: September 25, 2018)

Diffusion is the main limitation of storage time in spatially multimode applications of warm atomic vapors. Precise knowledge of diffusional decoherence in the system is desired for designing most of vapor memory setups. Here we present a novel, efficient and direct method of measuring unbiased diffusional decoherence, clearly distinguished from all other decoherence sources. We found the normalized diffusion coefficients of rubidium atoms in noble gases to be as follows: neon  $0.20 \text{ cm}^2/\text{s}$ , krypton  $0.068 \text{ cm}^2/\text{s}$  and we are the first to give an experimental result for rubidium in xenon:  $0.057 \text{ cm}^2/\text{s}$ . Our method consists in creating, storing and retrieving spatially-varying atomic coherence. Raman scattering provides a necessary interface to the atoms that allows for probing many spatial periodicities of atomic coherence concurrently. As opposed to previous experiments the method can be used for any single sealed glass cell and it does not require any setup alterations during the measurements and therefore it is robust and repeatable.

PACS numbers: 51.20.+d, 42.50.Hz, 42.50.Gy, 42.65.Dr

## I. INTRODUCTION

In recent years warm atomic ensembles have been widely used in many applications in quantum optics and atomic physics. The most promising applications include quantum repeaters [1], quantum memories [2] and ultra-precise magnetometry [3]. They have also been shown to be an effective medium for four-wave mixing processes [4], electromagnetically induced transparency (EIT) [5] and slow light generation [6].

An advantage of using warm atomic gas is undoubtedly simplicity of performing warm experiments and obtaining large optical depths. However, it entails fast thermal motion of atoms. Atomic motion limits the efficiency of many modern systems that use multimode properties of atomic ensembles. At best this motion can be slowed down and made diffusive by addition of a suitable buffer gas. Since diffusion is usually the main source of decoherence in multimode vapor memory systems, ability to measure and control its speed is highly desired. In particular it would be very useful to distinguish pure diffusional decoherence from other decoherence effects.

There is a number of currently developing systems where diffusion is the main limitation. An important example of such a system is storing and retrieving transverse modes and images in gradient echo memory [7–10], in collective Raman scattering [11] or in EIT [12]. Typically diffusional motion of atoms in a buffer gas limits the storage time [13, 14], restricts the number of spatial modes retrieved [11] or broadens the EIT spectrum [15]. Knowledge of the exact diffusion coefficient is particularly important for designing experiments with diffraction cancellation [12, 16–18]. Further progress would be significantly facilitated if one possessed convenient, robust and repeatable method for precise diagnostic of decoherence in the actual cell of a particular setup.

However, the available methods of measuring diffusion decoherence are indirect and require either variation of buffer gas pressure, prior knowledge of other sources of decoherence [19] or setup alterations within a single measurement [20, 21]. This makes them unsuitable for modern experiments where exact knowledge of diffusional decoherence of a single sealed glass cell in a specific setup is required.

Here we propose a novel, direct method which allows us to measure the diffusion in any given cell. The measurement provides more than enough data to verify its self-consistency and single out the diffusion from other motion-independent sources of decoherence. The method should be relatively easy to incorporate into a number of quantum memory setups.

As a demonstration we measure the diffusion coefficients of rubidium in neon, krypton and xenon in sealed glass cells at a pressure of a few torrs. These results will be useful for designing future experiments, since the data available till now is rather scarce and, most importantly, it was retrieved using indirect methods [19, 20, 22–28]. The data available for neon is inconsistent and that for krypton is hardly available [8, 27].

We also recommend using xenon as a buffer gas, for which we provide the very first experimental data as far as we know. Despite the latest applications of hyperpolarized xenon [29], the diffusion coefficient of rubidium in this gas has only been deduced from cross sections of velocity changing collisions [30] or interaction potentials [31].

This paper is organized as follows: in Sec. 2 we introduce the principles of our method, Sec. 3 describes in detail the experimental implementation, Sec. 4 contains the experimental results together with the reference data available. Finally, Sec. 5 concludes the paper.

---

\* radekch@fuw.edu.pl

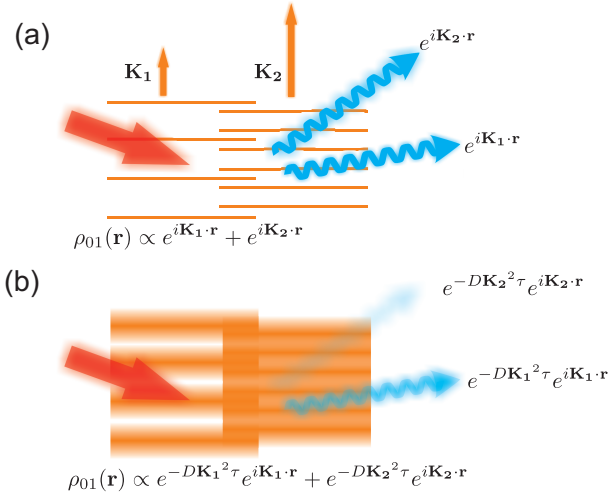


Figure 1. (Color online) (a) Planewave components of spatially dependent atomic coherence  $\rho_{01}(\mathbf{r})$  act as diffraction gratings deflecting laser beam at different angles. (b) Components of high periodicity are blurred faster due to diffusion, therefore the intensity of deflected light will decay faster for higher angles of deflection. During storage time  $\tau$ , the pattern component of specific periodicity corresponding to the wave vector  $\mathbf{K}$  blurs with decay rate  $DK^2$ , where  $D$  is the diffusion coefficient.

## II. METHOD

### A. General idea

Quantification of the diffusive motion of atoms using optical methods can be done in three general steps. At first a group of atoms has to be chosen and distinguished from others by changing their internal state. Then the atoms are let to spread due to diffusion in the absence of light. In the third stage one probes the group and observes the effects of the spread. This general scheme has various implementations [19, 20, 22–28] which typically consisted in exciting and probing a pencil-shaped atomic group using light beams. Instead here we create and, after a certain delay, probe patterns of spatially dependent atomic coherence  $\rho_{01}(\mathbf{r})$  between two long lived atomic levels  $|0\rangle$  and  $|1\rangle$ .

Patterns of atomic coherence are created through spontaneous (Stokes) Raman scattering. Each pattern comprises many plane-wave components with different periodicities. Those components decay at different rates due to diffusive motion of the atoms. After a certain storage time relative contribution of each plane-wave component can be measured by driving the anti-Stokes scattering. Then each plane-wave component acts as a diffraction grating deflecting driving laser beam as illustrated in Fig. 1 (a). By measuring the intensity of the anti-Stokes scattering light as a function of deflection angle and time between pattern creation and readout, we can calculate the decay rate of different plane-wave components constituting atomic coherence. We rely on the fact that in the

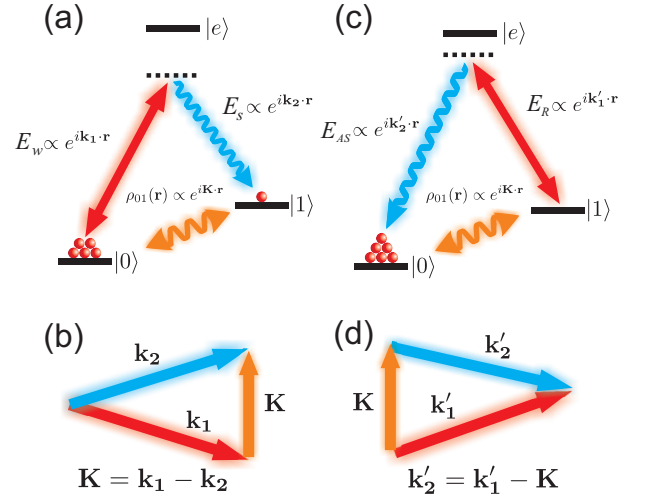


Figure 2. (Color online) (a) Atomic coherence  $\rho_{01}(\mathbf{r})$  is created in spontaneous Stokes scattering. (b) The difference between wave vectors of laser field  $\mathbf{k}_1$  and the scattering field component  $\mathbf{k}_2$  is stored in the spatially dependent phase of the atomic coherence. (c) Atomic coherence can be converted back to light in anti-Stokes scattering. (d) The atomic coherence phase is imprinted on anti-Stokes scattering as momentum conservation. Unlike the Stokes process, anti-Stokes scattering deterministically retrieves created coherence pattern on demand.

diffusion process periodic patterns of atomic coherence does not change their period but they are blurred over time as depicted in Fig. 1 (b). As atoms move, coherence at a specific point  $\mathbf{r}_0$  will reshuffle its values with the neighboring points. Evolution of atomic coherence in the dark will be described by the equation of diffusion with a coefficient  $D$  and homogeneous depolarization with a rate  $\gamma_0$  [7, 32]:

$$\frac{\partial}{\partial t} \rho_{01}(\mathbf{r}, t) = D \nabla^2 \rho_{01}(\mathbf{r}, t) - \gamma_0 \rho_{01}(\mathbf{r}, t). \quad (1)$$

This equation can be readily solved in Fourier domain:

$$\rho_{01}(\mathbf{r}, t) = e^{-\gamma_0 t} \sum_{\mathbf{K}} \beta(K) e^{-DK^2 t} e^{i\mathbf{K} \cdot \mathbf{r}}. \quad (2)$$

Evolution of each plane wave component of initial amplitude  $\beta(K)$  and wave vector  $K$  is described by a simple exponential decay at a rate  $\gamma(\mathbf{K}) = \gamma_0 + DK^2$ . As long as the evolution of  $\rho_{01}$  can be described by Eq. (1) with position-independent homogeneous depolarization with a rate  $\gamma_0$ , the measurement of decay rates  $\gamma(K)$  is sufficient to calculate  $D$  as a coefficient of the quadratic term of  $\gamma(K)$ .

### B. Creation and probing of atomic coherence

In Fig. 2(a) we illustrated the atomic levels involved in Stokes scattering leading to creation of coherence  $\rho_{01}(\mathbf{r})$

between levels  $|0\rangle$  and  $|1\rangle$ . Upon spontaneous scattering of a laser beam detuned from the  $|0\rangle \leftrightarrow |e\rangle$  transition both scattered light and atomic coherence are created. We shall consider a simple case where the laser beam and the scattered light are planewaves with wave vectors,  $\mathbf{k}_1$  and  $\mathbf{k}_2$ , respectively. The difference between the laser field wave vector  $\mathbf{k}_1$  and the created photons wave vector  $\mathbf{k}_2$  is accumulated in atoms as a spatial phase of atomic coherence. As illustrated in Fig. 2(b) the atomic coherence created will be of a form  $\rho_{01}(\mathbf{r}) = \beta e^{i\mathbf{K}\cdot\mathbf{r}}$ , where  $\mathbf{K} = \mathbf{k}_1 - \mathbf{k}_2$ .

Such periodic atomic coherence  $\rho_{01}(\mathbf{r})$  can work as a diffraction grating and deflect a laser beam. This is realized in anti-Stokes scattering process presented in Fig. 2(c) in which laser beam detuned from the  $|1\rangle \leftrightarrow |e\rangle$  transition is scattered at an angle. The spatial phase of atomic coherence  $\rho_{01}(\mathbf{r})$  is imprinted back onto the scattered photons as follows from Bragg condition. Provided driving laser beam is the plane wave with a wave vector  $\mathbf{k}'_1$ , the diffracted light wave vector will be  $\mathbf{k}'_2 = \mathbf{k}'_1 - \mathbf{K}$ , as illustrated in Fig. 2(d). Therefore by observing the intensity of the light  $I_{AS}(\theta)$  scattered at an angle  $\theta$ , we register a signal which is proportional to the modulus square of the corresponding plane wave component of atomic coherence  $|\beta(K) \exp(-\gamma(K)t)|^2$ , with  $\theta = K/k'_1 = K\lambda/2\pi$ .

### C. Averaging and retrieving the diffusion coefficient

Spatially varying atomic coherence  $\rho_{01}(\mathbf{r})$  is created in a spontaneous Stokes scattering process, which populates various planewave components randomly. Nonetheless, the average modulus square of the excitation amplitude  $\langle |\beta(K)|^2 \rangle$  created right after the scattering is set by the driving pulse parameters and can be kept constant between measurement series. Therefore, we can calculate the average intensity of the light scattered at a certain angle  $\theta = K/k'_1$  and for a given storage time  $\tau$ , incorporating Eq. (2):

$$\langle I_{AS}(\theta = K/k'_1, \tau) \rangle = \eta(K) \langle |\beta(K)|^2 \rangle e^{-2\gamma(K)\tau}, \quad (3)$$

where  $\eta(K)$  is efficiency of readout, *a priori* dependent on  $K$ . The only factor that depends on the diffusion time  $\tau$  is the intensity decay factor  $e^{-2\gamma(K)\tau}$ , which provides direct information about the decay rate  $\gamma(K)$ . Therefore for a given angle of observation  $\theta = K/k'_1$  we can infer  $\gamma(K)$  from an exponential fit to a series of experimental data taken for successive  $\tau$ .

By repeating the decay fits for many  $K$  we can gather and then fit the expected functional dependence  $\gamma(K) = \gamma_0 + DK^2$ , to obtain the diffusional coefficient  $D$ . In principle, we could use only two measurements of decay rates  $\gamma$  corresponding to just two different directions. Note that thanks to a particular way of populating spatially varying atomic coherence we create and probe many wave vectors concurrently without altering the setup. Thence

we obtain many points corresponding to a broad span of  $K$  vectors in a single measurement sequence, which provides for a robust quadratic fit of  $\gamma(K)$ . The quality and reliability of the experimental data is directly reflected in this last fit.

### D. Angular blurring at readout

So far we have assumed the driving beam to be a planewave. The finite size  $w$  of the driving laser beam in anti-Stokes scattering results in limited resolution in probing a wave vector space. The angular spread of the laser beam driving the readout will be transferred onto the angular distribution of the scattered light due to momentum conservation even for planewave atomic coherence  $\rho_{01}(\mathbf{r})$ . Thus for any specific angle of observation  $\theta = K/k'_1$  we detect the scattered light originating from several distinct Fourier components of the atomic coherence pattern. The contribution will come from the component of the wave vector  $K$  and its vicinity to the spread  $\sigma$ . We expect the spread  $\sigma$  to be of the order of the inverse of the driving laser beam size  $1/w$ .

The result of the limited resolution is an overall increase in the decay rates observed  $\gamma_{\text{obs}}$ . It can be estimated by convolving the storage time-dependent Fourier distribution of atomic coherence  $\rho_{01}(\mathbf{r})$  with a Gaussian of a spread  $\sigma$ , yielding:

$$\gamma_{\text{obs}}(K) = (\gamma_0 + 2D\sigma^2) + DK^2. \quad (4)$$

Note that the term quadratic in  $K$  in the above formula did not change, therefore the procedure of obtaining the diffusion coefficient  $D$  remains unchanged. We only have to assure that the term  $2D\sigma^2$  is small as compared to  $DK^2$ . This can be done by increasing the beam size  $w$ .

In conclusion all measurements can be completed by varying only one parameter – the diffusion time  $\tau$  equal to laser pulse separation while collecting scattered light on a camera. Data analysis require three straightforward steps: averaging, exponential fit and eventually quadratic fit to obtain  $D$ . This makes the whole procedure relatively quick and simple to repeat.

### E. Additional sources of decoherence

In Eq. (1) we assumed that decoherence could be divided into two types: the  $K$ -dependent diffusional type and the homogenous type. The latter originates mostly from atomic collisions. This division applies sufficiently to typical experimental conditions; however, other types of processes may contribute to decoherence as well.

In Eq. (1) we neglected the stray magnetic field. Taking such a field into account would require introducing an extra term in Eq. (1):  $i\mu_B(g_1m_1 - g_0m_0)B(\mathbf{r})\rho_{01}(\mathbf{r}, t)$  to represent additional, space-dependent build-up of the

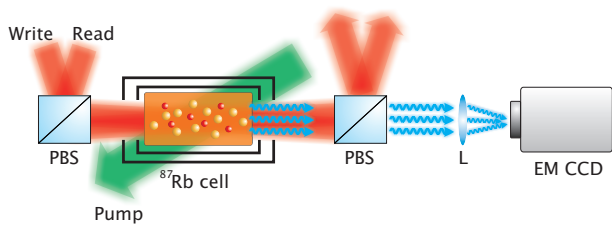


Figure 3. (Color online) Central part of the experimental setup. Rubidium-87 atoms are mixed with the buffer gas in a glass cell inside a double magnetic shielding. Pump, write and read are the laser beams used to prepare atoms in the ground state  $|0\rangle$ , to create and probe atomic coherence patterns respectively. Stokes and anti-Stokes scattering are singled out on a polarizing beam splitter PBS and observed in the far field on an electron multiplying EM CCD camera.

phase, where  $\mu_B g_i m_i$  is the magnetic moment for the  $i$ -th level. Nevertheless, we estimated that our final results would change only by 10% in the presence of a magnetic field gradient of 0.5 Gauss/mm or with a quadratically changing magnetic field of 10 mGauss/mm<sup>2</sup>. These values are considerably higher than in normal experimental conditions even without applying magnetic shielding.

We also noted that decoherence due to spin-exchange collisions might lead to quite complicated effects if  $\rho_{01}(\mathbf{r})$  was a fast varying function of position. These collisions could alter the state of the atoms at a different rate and at different points in space, leading to a nontrivial space dependence of  $\gamma_0$ . We calculated the rate of these collisions to be of the order of 1.5 kHz, which is negligible as compared to the diffusional decay caused by the atoms leaving the laser beams.

### III. EXPERIMENT

In our case the levels  $|0\rangle$  and  $|1\rangle$  between which we create atomic coherence  $\rho_{01}(r)$  are hyperfine split levels  $5_2S_{1/2}$ ,  $F=1$  and  $F=2$  respectively. Spatially dependent coherence  $\rho_{01}(r)$  is created and read with the use of Raman transitions between this levels. The scattered light is separated from much stronger stimulating lasers by a polarizer and additionally filtered out spectrally by a rubidium-85 filtering cell. The scattered light is registered by an electron multiplying CCD (Hamamatsu) camera sensor which is placed in the far field. The main part of the experimental setup is shown in Fig. 3, further details can be found in [11].

The operational sequence is shown in Fig. 4. Laser pulses were formed with the use of acousto-optical modulators. We began with optical pumping of rubidium atoms to the ground state  $F=1$ . The pump laser operates in resonance on the D2 line. Then we created random patterns of atomic coherence in the Stokes scattering process driven by 2-5  $\mu$ s pulses of the write laser detuned from the  $F=1 \rightarrow F'=1$  D1 transition line by 1 GHz to the red. The Stokes scattering was recorded with

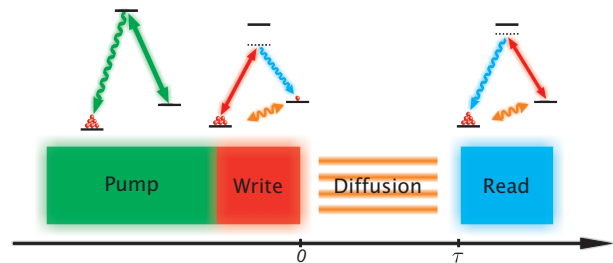


Figure 4. (Color online) Single operational sequence. First rubidium atoms are pumped on D2 line to  $F=1$  ground level  $|0\rangle$ . Then spontaneous Stokes scattering is driven to create spatially varying atomic coherence. Next the coherence is stored in the dark for a time  $\tau$  and we fades due to diffusion. Finally the coherence driving anti-Stokes scattering is probed.

a camera for diagnostic purposes. Next the atoms were left to diffuse for time  $\tau$ . Finally we used 5  $\mu$ s long pulses of read laser detuned 1 GHz from the  $F=2 \rightarrow F'=2$  D1 transition line to the blue to probe blurred atomic coherence  $\rho_{01}(\mathbf{r})$  and record anti-Stokes scattering intensity in the far field  $I_{AS}(\theta)$ .

Beam diameters  $1/e^2$  and powers for the Stokes and anti-Stokes drive laser were 5 mm, 4 mm and 16 mW, 7 mW respectively. They were chosen in order to achieve both good resolution as discussed above Eq. (4) and a sufficient scattering rate [11].

We repeated the create-store-read sequence multiple times and recorded random patterns of anti-Stokes scattering, changing the storage time  $\tau$ .

We used four rubidium-87 cells with different buffer gases. Those were: neon at the pressure of 2 Torr, krypton at 0.5 Torr and 1 Torr and xenon at 1 Torr. All cells were 10 cm long, 2.5 cm diameter cylinders made by Precision glassblowing. The longest times for anti-Stokes scattering observations were ca.  $\tau=50 \mu$ s, which corresponded to an RMS atomic displacement of about 1 mm, far less than the cell size.

The cells temperature was stabilized at ca. 70° C, which corresponded to an optical depth of 40 and a concentration of rubidium atoms  $n=10^{12} \text{ cm}^{-3}$ . Cells were heated with bifilar windings, but the heating current was interrupted for the time of impulse sequence inducing Raman scattering. The cells were placed inside a double magnetic shield. In the independent measurements we checked if the quality of our shielding is good and we estimated the decoherence rate due to imperfect shielding to be less than 1 kHz.

For each diffusion time  $\tau$  we averaged 500 images of anti-Stokes scattering each time obtaining smooth symmetric profiles. We subtracted the averaged background. Given that the most important thing for us is the intensity as a function of azimuth angle  $\theta$ , we also carried out a polar averaging around the laser beam direction increasing signal to noise ratio. The result of the measurements was average scattering intensity  $\langle I_{AS}(\theta, \tau) \rangle$  as a function of angle  $\theta$  and storage time  $\tau$ .

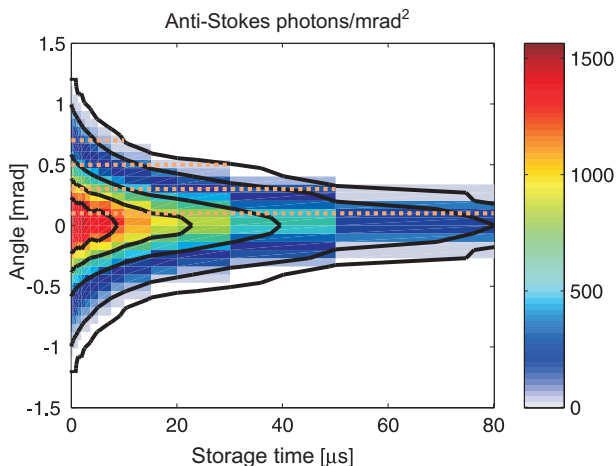


Figure 5. (Color online) Average number of photons per pixel  $\langle I_{AS}(\theta, \tau) \rangle$  in the anti-Stokes scattering process as a function of the storage time  $\tau$  and angle of observation  $\theta$ . Data taken for a cell with 1 Torr xenon. The decay is conspicuously faster for higher angles of scattering. The contour lines show 1200, 800, 400, 50, 10 photons per pixel.

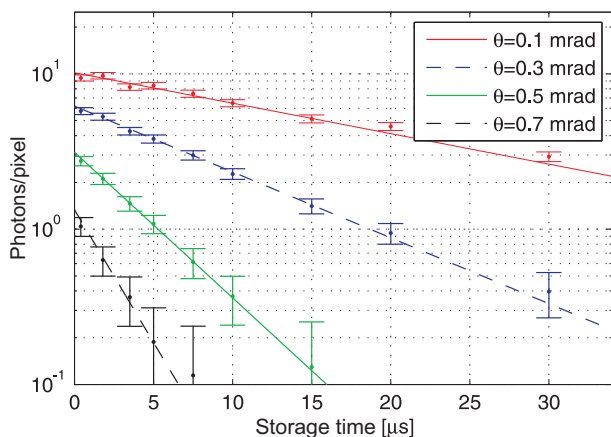


Figure 6. (Color online) Average number of photons per pixel  $\langle I_{AS}(\theta, \tau) \rangle$  as a function of the storage time  $\tau$  with exponential decay fits observed for four different angles  $\theta$ . The decays are visibly faster for higher scattering angles. The data corresponds to horizontal dashed lines in Fig. 5.

#### IV. RESULTS

In Fig. 5 we present a typical map of the averaged angular profiles of anti-Stokes scattering in cell with xenon vs free depolarization time  $\langle I_{AS}(\theta, \tau) \rangle$ . The results are given as a function of the scattering angle  $\theta$ , which is proportional to the wave vector of the corresponding Fourier components of atomic coherence patterns  $\theta = K\lambda/2\pi$ .

In Fig. 6 we plot an average number of photons as a function of the storage time  $\tau$  at a few angles  $\theta$  marked with dashed lines in Fig. 5. The decay rate is faster for higher angles of scattering. The error bars in Fig. 6 correspond to  $1\sigma$  uncertainty and were calculated from

the full statistics of camera counts. We fit exponential decays to the data taking the error bars into account. It is worth underlining that the data fits well to the curve at each scattering angle. As shown in Fig. 6, for high scattering angles  $\theta$  the average signal  $\langle I_{AS}(\theta, \tau) \rangle$  is at the level of one photon per shot which considerably increases the uncertainty of  $\gamma$ .

#### A. Diffusion coefficients

Having obtained an exponential fits for decays in all directions, we can analyze decays rates  $\gamma_{\text{obs}}(\theta)$  as a function of the deflection angle  $\theta$ . In Fig. 7(a) we present fitted decay rates for measurements in cells filled with 1 Torr of xenon as well as with 2 Torr of neon. In Fig. 7 (b) we give measured data for cells with krypton at two pressure values: 0.5 Torr and 1 Torr.

As expected, the data fits to the quadratic dependence  $\gamma_{\text{obs}}(\theta) = \gamma_{0,\text{obs}} + D\theta^2(2\pi/\lambda)^2$ . Now our  $1\sigma$  error bars correspond to respective confidence bound from the exponential fit. Note that for high decay rate values the uncertainties are large because they correspond to small and noisy signals.

The measurements described above were repeated several times in order to make sure the results were reliable and repeatable. We changed the amount of the light generated by altering pulse duration of the writing laser and by repeating measurements at different temperatures. The spread of diffusion coefficients obtained was about 5-12%, depending on the cell. We attribute this spread to the beam wander, laser power and frequency instability, and the drift of the temperature of the cell during each measurement sequence.

Buffer gas	Pressure [Torr]	$D[\text{cm}^2/\text{s}]$	$\gamma_{0,\text{obs}} [\text{kHz}]$
Ne	2	$91 \pm 11$	38
Kr	0.5	$136 \pm 9$	71
Kr	1	$57.5 \pm 3$	28
Xe	1	$52 \pm 3$	33

Table I. Fit parameters for measured cells. Temperature: 70° C.

In Tab. I we summarize fitted values from the measured data from charts in Fig. 7. Note, that for measurements in krypton the ratio of the obtained diffusion coefficients is close to the nominal pressure values.

To further verify the accuracy of our results, we carried out reference measurements for krypton at 1 Torr using write and read beams reduced ca. 3 times, so that their diameters  $1/e^2$  were 1.6 mm i 1.4 mm respectively. This time the measurement was definitely less accurate due to the spread of wave vectors of the read beam and due to aberrations in the imaging system. The diffusion coefficient measured lay within the range of 40  $\text{cm}^2/\text{s}$  to 65  $\text{cm}^2/\text{s}$ , which is consistent with other results.

Finally let us note, that the observed decay rate at  $K = 0$ ,  $\gamma_{0,\text{obs}}$  summarized in Tab. I is dominated by excessive

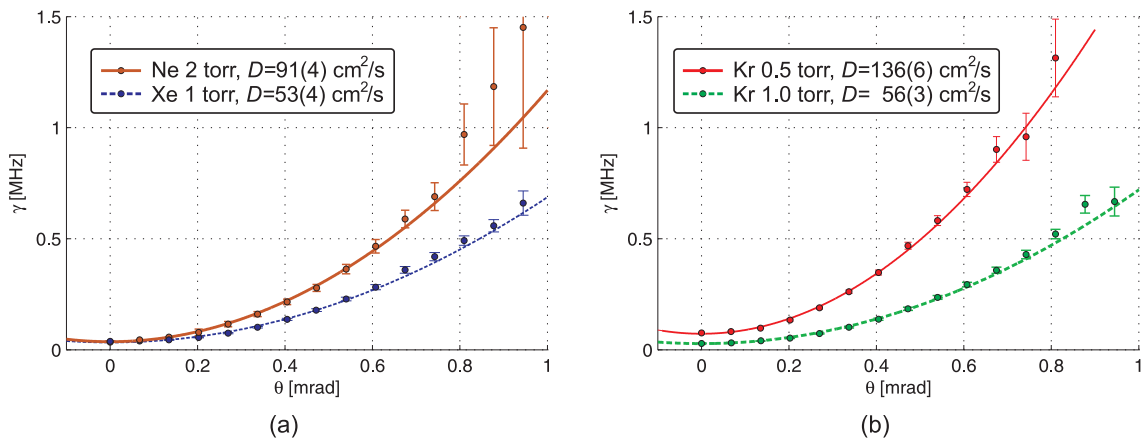


Figure 7. (Color online) Decoherence rates  $\gamma(\theta)$  as a function of the scattering angle corresponding to the atomic coherence wave vectors  $K = 2\pi\theta/\lambda$ . We fit the data with quadratic dependence  $\gamma_{\text{obs}}(\theta) = \gamma_{0,\text{obs}} + D\theta^2(2\pi/\lambda)^2$ . Quadratic term of fit gives the diffusion coefficient  $D$ . (a) Data taken for 1 Torr of xenon and 2 Torr of neon (b) Data taken for krypton of different pressures 0.5 Torr and 1 Torr.

contribution due to the finite read beam size,  $2D\sigma^2$  in Eq. (4). From respective collisional cross sections [25] we estimate ca. 1.5 kHz of decay rate due to Rb-Rb collisions and contributions less than 150 Hz from Rb – buffer gas collisions.

### B. Normalized diffusion coefficients

To compare our results with literature, we normalized the results to the standard conditions, i.e. at atmospheric pressure and at 0° C using the standard approximate formula [33], however strict scaling in a wide range of temperatures and pressures would involve Chapman-Enskog theory [34]

$$D_0 = D \left( \frac{P}{760 \text{ Torr}} \right) \sqrt{\frac{T_0}{T}}, \quad (5)$$

where  $P$  stands for the gas pressure at  $T_0 = 0^\circ\text{C}$ , and  $T$  is the temperature upon measurement. The diffusion coefficient will scale as  $T^{1/2}$  according to [35].

The temperature is known with good accuracy and the main error in determining  $D_0$  results from inaccuracy of gas pressure in cells, specified by the manufacturer not to be worse than 10%, and from the spread of the measured  $D$  values. The normalized diffusion coefficients are listed in Tab. II together with the data published previously.

The results we obtained do not differ from those obtained beforehand which – as we can see from Tab. II – were characterized by a noticeable spread.

## V. CONCLUSIONS

We have demonstrated a novel method for measuring diffusion coefficients of atoms tailored to atomic memory

applications. It should be emphasized that the method allows for singling out contribution of the diffusion in any given cell without prior knowledge of other decoherence mechanisms. It is based on creation of spatially varying atomic coherence fields, letting them diffuse in the dark and probing them. The fields comprise various spatial periodicities evolving concurrently, created and probed with Raman scattering. Due to the diffusion distinct components decay at different rates. All other significant sources of decoherence are homogenous and contribute equally to the decay of all components. Therefore we can extract diffusion coefficients by measuring decay rates for different periodicities of different components of spatially varying atomic coherence. Distinct components are conveniently mapped on different angles of the scattered light which enables observations with a camera in the far field.

Our method does not require any setup alterations within the measurement. This leads to quite direct determination of the diffusion coefficient founded on a basic time and angle calibrations of the experimental setup.

We have made sure that the method is accurate and repeatable. The results are based on multiple independent measurements for a number of various periodicities which give almost the same values. We also checked that varying laser beam widths and detunings does not affect the final result and that it scales properly with gas pressure.

We suppose that our method could be incorporated into experiments in which diffusion is the limiting factor, such as EIT, quantum memories including gradient echo memory or collective Raman scattering, by relatively straightforward modifications, such as adding a pump laser and a camera in the far field. Other technical requirements are typically fulfilled since these experiments also rely on using lasers of a few MHz frequency stability and magnetic shielding.



Buffer gas	$D_0[\text{cm}^2/\text{s}]$ – this paper	$D_0[\text{cm}^2/\text{s}]$ - previous results
Ne	$0.20 \pm 0.02$	0.11 [13], 0.18 [28], 0.31 [19, 24], 0.48 [25]
Kr	$0.068 \pm 0.006$	0.1 [27] 0.04 [8]
Xe	$0.057 \pm 0.007$	No experimental data

Table II. Measured diffusion coefficients of rubidium atoms in noble buffer gases: Ne, Kr, Xe. The results are normalized to 0°C and 760 Torr pressure.

We have measured diffusion coefficients of rubidium in neon, krypton and xenon. Reliable values of diffusion coefficients in these gases facilitate setup design and data interpretation in the multimode quantum storage experiments. Moreover we recommend the use of xenon as a buffer gas in case of Raman interaction and, to the best of our knowledge, we provide the first experimental value of diffusion coefficient in this gas. We believe that this value can also help develop experiments with hyperpolarized xenon.

## VI. ACKNOWLEDGMENTS

We acknowledge the generous support from Konrad Banaszek and Rafał Demkowicz-Dobrzański. This work was supported by the Foundation for Polish Science TEAM project, EU European Regional Development Fund and FP7 FET project Q-ESSENCE (Contract No. 248095), National Science Centre grant no. DEC-2011/03/D/ST2/01941 and by Polish NCBiR under the ERA-NET CHIST-ERA project QUASAR.

- 
- [1] L. M. Duan, M. D. Lukin, J. I. Cirac, and P. Zoller, *Nature* **414**, 413 (2001).
- [2] J. Appel, E. Figueroa, D. Korystov, M. Lobino, and A. Lvovsky, *Phys. Rev. Lett.* **100**, 093602 (2008).
- [3] W. Chalupczak, R. M. Godun, S. Pustelny, and W. Gawlik, *Applied Physics Letters* **100**, 242401 (2012).
- [4] C. F. McCormick, V. Boyer, E. Arimondo, and P. D. Lett, *Optics letters* **32**, 178 (2007).
- [5] M. Fleischhauer, A. Imamoglu, and J. Marangos, *Reviews of Modern Physics* **77**, 633 (2005).
- [6] A. B. Matsko, O. Kocharovskaya, Y. Rostovtsev, G. R. Welch, A. S. Zibrov, and M. O. Scully, *Advances In Atomic, Molecular, and Optical Physics* **46**, 191 (2001).
- [7] Q. Glorieux, J. B. Clark, A. M. Marino, Z. Zhou, and P. D. Lett, *Optics Express* **20**, 12350 (2012).
- [8] D. Higginbottom, B. Sparkes, M. Rancic, O. Pinel, M. Hosseini, P. Lam, and B. Buchler, *Phys. Rev. A* **86**, 023801 (2012).
- [9] J. B. Clark, Q. Glorieux, and P. D. Lett, *New Journal of Physics* **15**, 035005 (2013).
- [10] X. W. Luo, J. J. Hope, B. Hillman, and T. M. Stace, *Phys. Rev. Lett.* **111**, 110401 (2013).
- [11] R. Chrapkiewicz and W. Wasilewski, *Optics Express* **20**, 29540 (2012).
- [12] O. Firstenberg, M. Shuker, A. Ron, and N. Davidson, Pre-print arXiv:1207.6748 (2012).
- [13] M. Shuker, O. Firstenberg, R. Pugatch, A. Ron, and N. Davidson, *Physical Review Letters* **100** (2008), 10.1103/PhysRevLett.100.223601.
- [14] P. K. Vudyasetu, R. M. Camacho, and J. C. Howell, *Physical Review Letters* **100** (2008), 10.1103/PhysRevLett.100.123903.
- [15] M. Shuker, O. Firstenberg, R. Pugatch, A. Ben-Kish, A. Ron, and N. Davidson, *Phys. Rev. A* **76**, 023813 (2007).
- [16] O. Firstenberg, M. Shuker, R. Pugatch, D. Fredkin, N. Davidson, and A. Ron, *Physical Review A* **77**, 043830 (2008).
- [17] O. Firstenberg, P. London, M. Shuker, A. Ron, and N. Davidson, *Nature Phys.* **5**, 665 (2009).
- [18] D. Yankelev, O. Firstenberg, M. Shuker, and N. Davidson, *Optics letters* **38**, 1203 (2013).
- [19] W. Franzen, *Physical Review* **115**, 850 (1959).
- [20] P. Bicchi, L. Moi, P. Savino, and B. Zamboni, *Il Nuovo Cimento B* **55**, 1 (1980).
- [21] D. Glassner, B. Ai, and R. Knize, *Physical Review A* **54**, 3335 (1996).
- [22] R. A. Bernheim, *The Journal of Chemical Physics* **36**, 135 (1962).
- [23] R. J. McNeal, *The Journal of Chemical Physics* **37**, 2726 (1962).
- [24] M. Arditi and T. Carver, *Physical Review* **136**, A643 (1964).
- [25] F. Franz, *Physical Review* **139**, A603 (1965).
- [26] A. Gozzini, N. Ioli, and F. Strumia, *Il Nuovo Cimento B Series 10* **49**, 185 (1967).
- [27] M. A. Bouchiat, *The Journal of Chemical Physics* **56**, 3703 (1972).
- [28] J. Vanier, J.-F. Simard, and J.-S. Boulanger, *Physical Review A* **9**, 1031 (1974).
- [29] A. Fink, D. Baumer, and E. Brunner, *Physical Review A* **72**, 053411 (2005).
- [30] K. Gibble and A. Gallagher, *Phys. Rev. A* **43**, 1366 (1991).
- [31] W. A. Hamel, J. E. M. Haverkort, H. G. C. Werij, and J. P. Woerdman, *Journal of Physics B: Atomic and Molecular Physics* **19**, 4127 (1986).
- [32] I. Lowe and S. Gade, *Physical Review* **156**, 817 (1967).
- [33] W. Happer, *Reviews of Modern Physics* **44**, 169 (1972).
- [34] S. Chapman and T. G. Cowling, *The Mathematical Theory of Non-uniform Gases: An Account of the Kinetic Theory of Viscosity, Thermal Conduction and Diffusion in Gases* (Cambridge University Press, Cambridge, 1970) p. 423.
- [35] W. Hogervorst, *Physica* **51**, 59 (1971).